Effect of defocus on laser-coupling into gold cones

Contact iab500@york.ac.uk

I. Bush, L. Gartside and J. Pasley
Department of Physics, University of York, Heslington, York, YO10 5DD, UK

J. Green, M. Notley, H. Lowe, C. Spindloe, T. Winstone, F. Cameron and R. Clarke
Central Laser Facility, STFC, Rutherford Appleton Laboratory, HSIC, Didcot, Oxon OX11 0QX, UK

T. Ma, T. Yabuuchi, M. Wei and F. N. Beg
Department of Mechanical and Aerospace Engineering, University of California San Diego, La Jolla, California 92093-0411, USA

A. MacPhee, A. J. MacKinnon and M. H. Key
Lawrence Livermore National Laboratory, Livermore, California 94550-9234, USA

R. B. Stephens
General Atomics, San Diego, California 92121-1122, USA

W. Nazarov
University of St. Andrews, School of Chemistry, St. Andrews, KY16 9AJ, UK

Introduction

Fast ignition is an inertial confinement fusion scheme in which a separate short-pulse laser is used to heat a compressed sphere of deuterium-tritium (DT) fuel to the point of ignition[1]. In re-entrant cone-guided fast ignition a gold cone is inserted into the DT fuel to create a path for the igniter laser. The igniter laser energy couples to the tip of the cone producing a current of hot electrons, which heats the pre-compressed fuel. Getting good energy coupling from the igniter laser into hot electrons is therefore of key importance in re-entrant cone guided fast ignition.

The beam enters the cone through the open end, along the axis of the cone, so that it irradiates the inside tip of the cone. The position of the focus however can be moved to before or after the cone tip to change the profile of the irradiated area. A recent experiment on the Titan Laser at Lawrence Livermore National Laboratory[2] showed enhanced emission from copper cone targets in a thermoluminescent dosimeter diagnostic[3] for the case where the laser is focused beyond the tip of the cone. The motivation behind this Vulcan Petawatt experiment was to build upon this data and determine the effect of defocus on the laser-coupling into hot electrons for cone targets.

Targets

Gold cone targets were used for the experiment, as shown in figure 1, which were manufactured on site. The gold cones had 20 µm thick walls, were 1.5 mm long with a 20° half-angle. The tip of the cone was 30 µm in diameter was 6 µm thick.

Attached to each cone used in the experiment was a 1 mm long copper wire, 40 µm in diameter, to be used as a diagnostic for the hot electrons emitted from the cone tip[4, 5]. Some of the cones were coated in copper on the inside, to a thickness of between 2.0 and 2.6 µm. In total over 50 cones were fielded during the experiment.

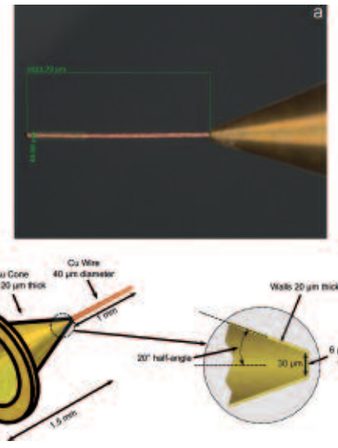

Figure 1. Gold cone-wire targets used in the experiment. a – photograph of copper wire attached to gold cone. b – diagram showing dimensions of cone.

Experimental setup

Vulcan Petawatt is a 1053 nm neodymium glass laser. In this experiment laser pulses lasted 0.5 – 2 ps. Shot energies were 600 ± 100 J, focused using an f/3 parabolic mirror to an 8 µm (FWHM) spot, giving a peak intensity of ~ 10^{21} W cm^{-2}. As with all high power laser systems, Vulcan Petawatt has an intrinsic prepulse. This lasts for ~1 ns, with an intensity contrast of ~10^{-7} and an energy contrast of ~10^{-4}.

There were three Cu-K_α diagnostics fielded; a 2D crystal imager, a pair of HOPG (highly oriented pyrolitic graphite) spectrometers and a single photon counting CCD camera. The other primary diagnostic used was an optical probe. An electron spectrometer and a pair of X-ray pinhole cameras were also fielded.

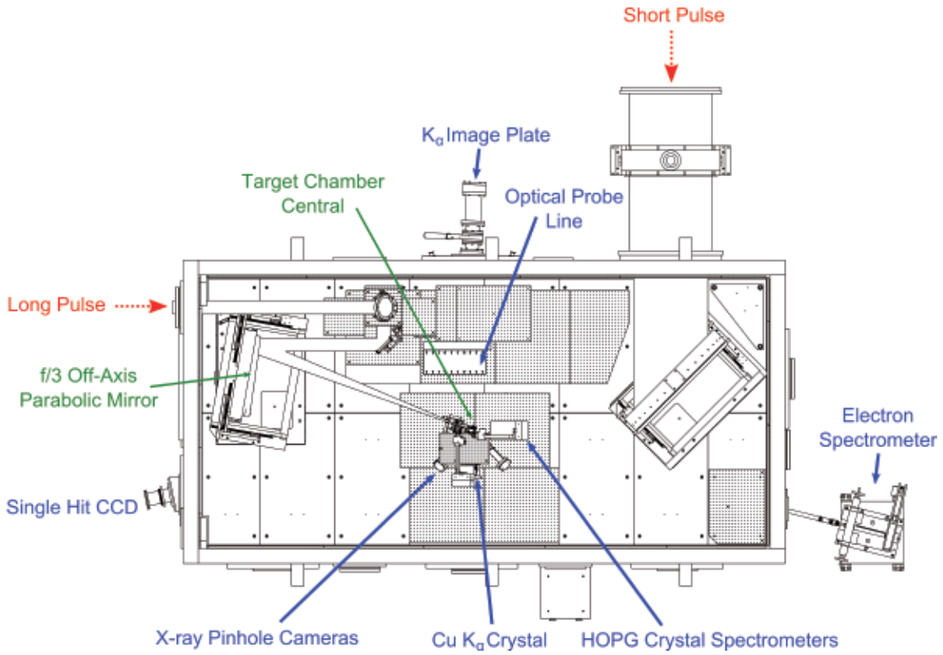

Figure 2. Vulcan Petawatt target chamber layout.

The Cu K_α imager was a Bragg reflecting quartz SiO_2 (2131) crystal, apertured to a 20 mm diameter. The crystal had a radius of curvature of 500 mm and was placed, looking side on, 281 mm from the target. This gave an 8 times magnification. The lattice spacing for the crystal is 3.082 Å, giving a Bragg angle of 88.7° for Cu K_α emission at 8.05 keV. The X-ray emission was recorded on to Fujifilm BAS-SR image plates.

The HOPG spectrometers fielded were based upon Bragg reflecting crystals with a mosaic spread of 0.4 ± 0.1° (ZYA)[6]. The spectrum was also recorded on to Fujifilm BAS-SR image plates, with a spectral range of 0.8 keV, centered at 7.9 keV The spectrometers were able to resolve both $K_{\alpha1}$ (8.05 keV) and $K_{\alpha2}$ (8.03 keV) lines, with a spectral resolution of 0.5 eV. Both HOPG spectrometers were positioned above the target.

The single photon counting camera used was a Princeton Instruments SX1300 camera. The pixel size was 20 µm × 20 µm, with a total area of 1300 × 1340 pixels. Filtering was used such that only single photons would hit each pixel. The use of a single photon counting camera in this way allows absolute K_α yields from the copper wire to be determined.

The optical probe worked at 2ω, delayed 400 ps to the main pulse. The view was side-on to the target, perpendicular to the direction of the laser. Channels for shadowgraphy and interferometry were used, to measure the extent of the expansion of plasma around the cone. The interferometry channel can be used to determine the density of plasma being emitted from the cone.

The position of the other diagnostics and layout of the target chamber are shown in figure 2.

Experimental Data from Diagnostics

All the examples from the diagnostics in this section are from the same shot, a plain cone (no copper coating), with the laser focused 400 µm past the cone tip.

Figure 3 shows an image plate scan and lineout along the wire for the Cu K_α imager, with the background subtracted on the lineout. An exponential fall-off along the wire can be seen, with a slight brightening again towards the end of the wire. The length over which the emission takes to decay (for example to fall to 1/e of its peak value) is related to the energy spectrum of the electrons, with hotter electrons penetrating further down the wire. The K_α line frequency shifts at higher temperatures, decreasing the collection efficiency of the K_α imaging crystal[7]. This means that care must be taken in looking at integrated K_α yields from the imaging crystal, as the signal level on the image plate is not directly proportional to the emission intensity.

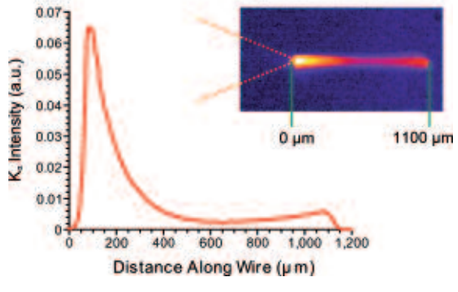

Figure 3. Copper K_α imager emission along wire.

In figure 4 a lineout from the HOPG spectrometer is shown, along with the image plate scan the lineout was generated from. The $K_{\alpha1}$ and $K_{\alpha2}$ lines are resolvable individually with the $K_{\alpha1}$ peak having the brighter emission. The signal intensity on the two HOPG spectrometers have very good agreement, and the correlation between the integrated signal from the K_α imager and integrated spectrum from the HOPG spectrometers is shown in figure 8.

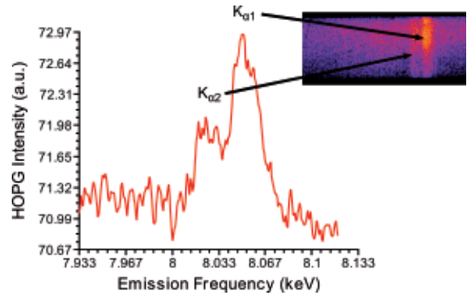

Figure 4. HOPG crystal spectrometer emission, showing $K_{\alpha1}$ and $K_{\alpha2}$ peaks.

Figure 5 shows the images taken from the optical probe, before the shot and at 400 ps. This shows the low magnification shadowgraphy channel and the interferometry channel. The graph shows the extent of the plasma expansion around the wire. This data will be used to reconstruct initial temperature profiles by comparison with radiation hydrodynamic modelling.

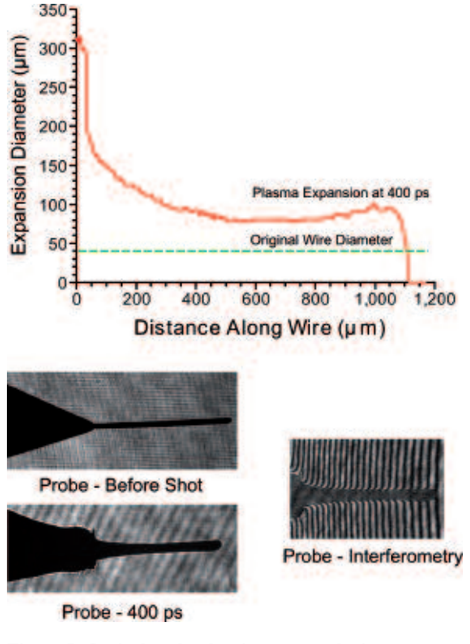

Figure 5. Optical probe showing cone and wire expansion 400 ps after main pulse. Images from the shadowgraphy and interferometry channels for the probe are shown.

Experimental results and discussion

In figure 6 some preliminary results are shown, comparing the defocus position with the intensity of the integrated spectrum from the HOPG spectrometers. First the background level was subtracted, and then the area under the lineout for $K_{\alpha1}$ and $K_{\alpha2}$ peaks found. The values are also normalised to laser energy. The negative values on the x-axis are for configurations were the laser is focused before the cone tip, and the positive values were the laser is focused past the cone tip. The highest signal from the HOPG can be seen when the laser is not focused tightly to the cone tip. These plots show the results from all of the bare cones (no Cu coating) that were shot.

Figure 7 shows the variation in 1/e length for the various defocus positions. This is the length over which the signal decreases from the peak, to 1/e of this value (c.f. figure 3). It appears that the scale length decreases in the case where the laser is defocused, which suggests a colder electron energy spectrum.

A preliminary comparison between the signal from the HOPG spectrometers (the same values as shown in figure 6) and the K_α imager is shown in figure 8. The signal from the K_α imager has been corrected for the background level, as shown in figure 3, and once again normalised to laser energy. To avoid the effects of the intensity of the K_α emission brightening towards the far end of the wire the signal is integrated over the first 250 µm only, from the peak of the emission.

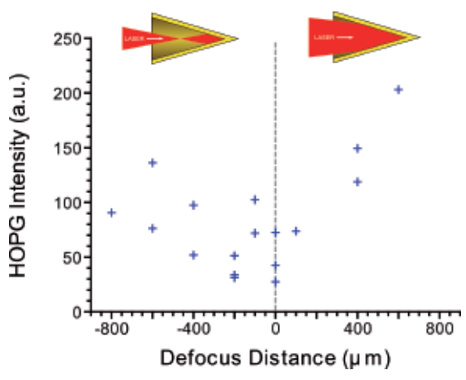

Figure 6. Variation of HOPG spectrometer integrated signal intensity with defocus position.

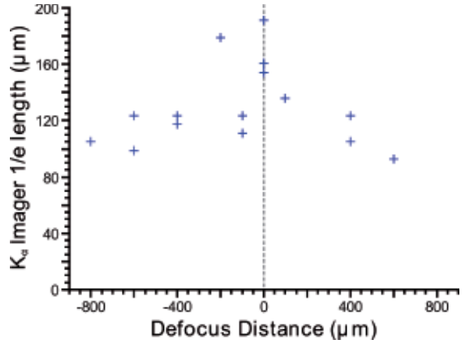

Figure 7. 1/e length variation with defocus for the K_α imager.

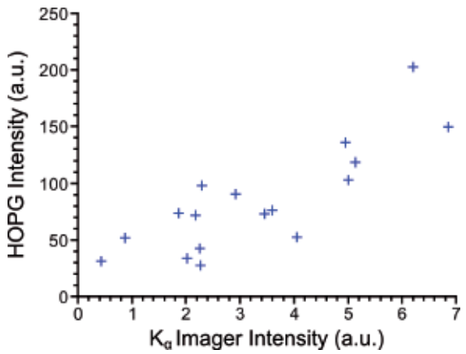

Figure 8. Integrated HOPG spectrum intensity vs. K_α imager intensity integrated along the length of the wire.

Conclusions

The preliminary analysis of the data from this experiment suggests defocusing of the laser into the cone-wire targets, by up to 800 μm, appears to enhance the laser energy coupling into the cone. This could be due to defocusing leaving the cone intact during the prepulse. Modelling is being undertaken to determine if this effect could be responsible for the high Cu K_α yields in the defocused cases. Care must be taken in applying these results to a full scale FI system, where the energy in the prepulse will be much higher.

Acknowledgements

The authors wish to gratefully acknowledge the assistance of the staff at the Central Laser Facility, STFC Rutherford Appleton Laboratory.

References

1. M. H. Key, *Phys. Plasmas* **14**, 055502 (2007).
2. L. Van Woekrom *et al*., *Phys. Plasmas* **15**, 056304 (2008).
3. R. J. Clarke *et al*., *J. Radiol. Prot*. **26**, 277 (2006).
4. R. Kodama *et al*., *Nature* **432**, 1005 (2004).
5. J. A. King *et al*., *Phys. Plasmas* **16**, 020701 (2009).
6. A. Pak *et al*., *Rev. Sci. Instrum*. **75**, 3747 (2004).
7. K. U. Akli *et al*., *Phys. Plasmas* **14**, 023102 (2007).